A CRISPR/Cas9-based screening for non-homologous end joining inhibitors reveals ouabain and penfluridol as radiosensitizers

Jie Du[1], Jun Shang[1], Fei Chen[1], Yushuo Zhang[1], Narui Yin[1], Ting Xie[1], Haowen Zhang[1], Jiahua Yu[1] and Fenju Liu[1]

[1]Department of Radiobiology, School of Radiation Medicine and Protection, Medical College of Soochow University. School for Radiological and Interdisciplinary Sciences (RAD-X), Soochow University. Collaborative Innovation Center of Radiological Medicine of Jiangsu Higher Education Institutions. Jiangsu Provincial Key Laboratory of Radiation Medicine and Protection, Suzhou, China.

Running title: Screening for NHEJ inhibitors

Keywords: non-homologous end joining, CRISPR/Cas9, high-resolution melting analysis, screening, radiosensitizer

Corresponding Author: Fenju Liu, School of Radiation Medicine and Protection, Medical College of Soochow University, Suzhou 215123, China. Phone: 86-0512-65880060; Fax: 86-0512-65884830; E-mail: radiobiology@126.com. Jiahua Yu, School of Radiation Medicine and Protection, Medical College of Soochow University, Suzhou 215123, China. Phone: 86-0512-65880065; Fax: 86-0512-65884830; E-mail: yujiahua@suda.edu.cn

Financial information: This work was supported by Natural Science Foundation of China (grand numbers 31270897 to F. Liu, 81271682 to F. Liu and 81202149 to J. Yu).

Abstract

Non-homologous end joining (NHEJ) is the major pathway responsible for the repair of ionizing radiation (IR)-induced DNA double-strand breaks (DSBs), and correspondingly regulates the cellular response to IR. Identification of NHEJ inhibitors could substantially enhance the tumor radiosensitivity and improve the therapeutic efficiency of radiotherapy. In present study, we demonstrated a screening for NHEJ inhibitors by using the clustered regularly interspaced short palindromic repeats (CRISPR)/CRISPR-associated protein 9 (Cas9) system and high-resolution melting (HRM) analysis. Since NHEJ is regarded as an error-prone mechanism, the NHEJ-mediated ligation of the site-specific DSB induced by Cas9 nuclease would eventually cause the mutation of the targeted sequence. Then, HRM analysis, a reliable and rapid assay for detecting sequence variation, was performed to evaluate the mutation efficiency of the targeted site. Validating analysis confirmed the NHEJ activities was positively correlated with the mutation frequencies. Next, an approved drug library containing 1540 compounds was interrogated by using this screening strategy. Our results identified ouabain, a cardiotonic agent, and penfluridol, an antipsychotic agent, have the capacity to restrain NHEJ activity. Further experiments in vitro revealed the radiosensitizing effects of these compounds. Overall, we presented a cell-based screening for NHEJ inhibitors which could promote the discovery of novel radiosensitizers.

Introduction

Induction of DNA double-strand breaks (DSBs) is one of the fundamental mechanisms by which ionizing radiation (IR) and chemotherapeutic drugs exert their cytotoxic effects on tumor cells (1-3). DSBs could also be generated in response to a plethora of endogenous and exogenous genotoxic agents (4,5). DSB is generally regarded as the most dangerous type of DNA lesion, since one single unrepaired DSB is sufficient to initiate programmed cell death (6). To counteract the threat of DSB and maintain genome integrity, cells have evolved an elaborate network to coordinate the lesion recognition, signal transmission, cell cycle synchronization and damage restoration (7). In eukaryotic cells, there are two major mechanisms of DSB repair: homologous recombination (HR) and non-homologous end joining (NHEJ) (3,8). HR is an error-free repair pathway and requires the intact sequence information from the sister chromatid, thus its function is believed to restrict during S and G2 phases of the cell cycle when the homologous template is available. Unlike HR, NHEJ can operate throughout the cell cycle and work in a template-independent manner. NHEJ involves the direct processing and religation of the broken ends, which could result in deletion or insertion of the nucleotides. Though NHEJ is inaccurate, it is estimated to repair up to 85% of IR-induced DSBs in the mammalian cells (9-11).

The proficiency of DSB repair in tumor cells mainly, if not all, determines the sensitivity to IR-induced cytotoxicity. Therefore, targeting DSB repair pathway might hold the promise for improving the outcome of cancer radiotherapy (1-3,12). Indeed, increasing efforts have been invested in discovering DSB repair inhibitors, particularly the small molecules that could suppress the effector proteins involved in HR and NHEJ. To name a few, NU7441 and CC-115, inhibitors of DNA-dependent protein kinase catalytic subunit (DNA-PKcs) (13,14), KU55933 and CP466722, inhibitors of ataxia-telangiectasia mutated (ATM) (15,16), olaparib and rucaparib, inhibitors of poly(ADP-ribose) polymerase (17,18), have been identified to inhibit DSB repair and substantially increase the anti-tumor activity of IR.

Currently, the targeted genome editing technology has brought a revolutionary surge in life science, especially the clustered regularly interspaced short palindromic repeats (CRISPR)/CRISPR-associated protein 9 (Cas9) system, originally discovered as an adaptive immune system of bacteria and archaea to defend themselves against viral infection (19,20). Cas9 nuclease monomer is able to induce a site-specific DSB by the direction of a customized single guide RNA (sgRNA), hence desired gene knockin or knockout could be easily accomplished by DSB repair through HR or NHEJ. Here, we used the CRISPR/Cas9 system to produce a DSB in the gene loci of hypoxanthine guanine phosphoribosyltransferase (HPRT) or heparin binding epidermal growth factor like growth factor (HBEGF), and analyze their mutation frequencies which could reflect the NHEJ activity. In order to rapidly and quantitatively evaluate the mutation frequencies, high-resolution melting (HRM) analysis, a simple PCR-based method for detecting DNA sequence variation, was performed following the NHEJ repair of the Cas9 nuclease-mediated DSB. HRM analysis relies on saturating dye, such as EvaGreen and LCGreen, instead of SYBR Green, and it is so sensitive that even a single nucleotide variant could be identified (21,22).

In present study, by taking advantage of CRISPR/Cas9 system and HRM analysis, a cost-effective screening method for NHEJ inhibitors has been developed. Validation of this novel method demonstrated the satisfactory sensitivity and reliability to quantitate the CRISPR/Cas9-induced mutation, as well as the suppressive effects of DNA-PKcs inhibitors on NHEJ activity. Next, an approved drug library was screened, and a collection of compounds were identified to impair NHEJ activity. Further experiments in vitro verified the suppressive effects on DSB repair and the radiosensitizing function of these drugs. Our results revealed ouabain, a cardiotonic agent, and penfluridol, an antipsychotic agent, might be potential candidates as radiosensitizers.

Materials and Methods

Cell culture and chemical reagents

HEK293T and HeLa cells were obtained from the Cell Bank of the Chinese Academy of Sciences (Shanghai, China) in September, 2015. T98G cells were obtained from American Type Culture Collection in November, 2015. All the cell lines were characterized by Genetic Testing Biotechnology Corporation (Suzhou, China) using short tandem repeat (STR) markers. These cells were cultured in Dulbecco's Modified Eagle Medium (DMEM) supplemented with 10% fetal bovine serum (Hyclone, Logan, UT). NU7441 and KU-0060648 were purchased from Selleck Chemicals (Houston, TX) and dissolved in dimethyl sulfoxide (DMSO) to obtain a stock solution, stored at -20°C and diluted to the desired concentration in fresh medium immediately before use.

DNA vector preparation and transfection

Cas9/sgRNA expressing vector construction kit was obtained from ViewSolid Biotech (Beijing, China). The sgRNA against HPRT (sgHPRT) or HBEGF (sgHBEGF) were inserted into the pre-linearized vector according to the manufacturer's instruction. The sequences of sgHPRT and sgHBEGF were shown in Fig. 1A and S1A (23,24). CRISPR/Cas9 plasmids were transfected into cells using Lipofectamine 2000 Reagent (Invitrogen, Carlsbad, CA).

Genomic DNA extraction

For cells cultured in dishes, genomic DNA was extracted by MiniBEST Universal Genomic DNA Extraction Kit (Takara Bio, Otsu, Japan). For cells cultured in 96-well plates, genomic DNA extraction was performed by using Chelex-100 ion exchange resin (Sigma, St. Louis, MO). Briefly, cells in each well were lysed in 200 μl 5% (w/v) Chelex-100 suspension in deionized water containing 0.2 mg/ml proteinase K. Then the lysates were incubated at 56ºC for 30 min, subsequently at 95ºC for 10 min, and vigorously vortexed for 10 seconds. After centrifuge at 12, 000

× *g* for 5 min, the supernatant containing genomic DNA was collected for further analysis.

Polymerase chain reaction (PCR) and T7 endonuclease 1 (T7E1) assay

CRISPR/Cas9 plasmid targeted site was amplified from 100 ng genomic DNA by using PCR Master Mix (Thermo Fisher Scientific, Waltham, MA). Primer sequences were: forward 5'-ATCCAATCAAATGTTTGTATCCTGT-3'; reverse 5'-CCCTTCAATGTTTACTTTGTTCTGG-3'. PCR thermal cycling conditions were 1 cycle at 95°C for 2 min; 35 cycles at 95°C for 30 sec, at 53°C for 30 sec, at 72°C for 40 sec; and 1 cycle at 72°C for 10 min. Next, the PCR amplicons were denatured at 95°C for 5 min, and annealed to allow the heteroduplex formation by cooling down to 75°C for 20 min and to 15°C for 30 min. Finally, the heteroduplex products were digested by 5 units of T7E1 (ViewSolid Biotech) at 37°C for 30 min, and immediately subjected to 2% agarose gel electrophoresis.

HRM analysis

HRM analysis premix (containing hot start Taq DNA polymerase, dNTPs, EvaGreen dye, HRM PCR buffer and ROX reference dye) was obtained from Tiangen Biotech (Beijing, China). Primer sequences for HPRT were: forward 5'-AGGTTATGACCTTGATTTATTTTGCA-3'; reverse 5'-AACAGCTGCTGATGTTTGAAATTAA-3'. Primer sequences for HBEGF were: forward 5'-TGGGCGGGTGTCTGATG-3'; reverse 5'-CAGCTGGTCCGTGGATACAGT-3'. The real-time PCR reaction mixture consisted of 20 ng genomic DNA, 200 nM forward and reverse primers, and HRM analysis premix in a final volume of 20 µl. Real-time reaction was run in 96-well plates by using ViiA 7 Real-time PCR System (Applied Biosystems, Foster City, CA). The thermal cycling conditions were: 95°C for 2 min; 40 cycles at 95°C for 15 sec, 60°C (HPRT locus) or 61°C (HBEGF locus) for 1 min. The PCR amplicons were then denatured at 95°C for 15 sec and annealed at 60°C for 1 min, followed by gradually

temperature elevation from 60°C to 95°C by 0.02°C/sec increment. The fluorescent data were continuously acquired during the slow DNA melting process.

HRM data analysis were performed as previously described (25,26). The exponential background subtraction method was applied to normalized raw fluorescent data. Next, the melting curves were converted into a subtractive plot in which the relative fluorescence difference (ΔF) to a control curve against temperature were shown. Finally, the maximum value of ΔF (ΔF_{max}) was used to determine the mutation frequency of the CRISPR/Cas9 plasmid-induced NHEJ.

Approved drug library screening

Approved drug library containing 1540 compounds was obtained from TargetMol (Boston, MA) and supplied as pre-dissolved DMSO solution with the concentration of 10 mM. HEK293T cells were transfected with CRISPR/Cas9 plasmid for 5 h, then the cells were trypsinized and seeded in 96-well plates. The approved drugs were added in a final concentration of 5 μM. After 24 h, the genomic DNA was extracted for HRM analysis. The quality of the screening was evaluated by Z' factor, defined as $1 - [3 (\sigma_{c+} + \sigma_{c-}) / |\mu_{c+} - \mu_{c-}|]$ (27), where σ_{c+} and σ_{c-} are the standard deviations of the ΔF_{max} of the NU7441 and DMSO-treated samples, and μ_{c+} and μ_{c-} are the means of the ΔF_{max} of the NU7441 and DMSO-treated samples.

Cell viability assay

After treated with indicated conditions, cells were incubated with 10 μl CCK-8 solution at 37°C for 2 hours. The absorbance was measured at 450 nm using a spectrophotometer.

NHEJ and HR reporter plasmid assay

NHEJ or HR activities were measured by using NHEJ or HR reporter plasmid as previously described (28,29). Briefly, the plasmids were digested with I-SceI enzyme (New England Biolabs, Ipswich, MA) and then co-transfected with pCMV-DsRed plasmids into HEK293T cells using Lipofectamine 2000 Reagent. Successful NHEJ

or HR reconstitutes the functional GFP gene, and GFP positive cells were quantified by flow cytometry (BD Biosciences, San Jose, CA). The red fluorescence served as an internal control for transfection efficiency. The ratio of GFP positive cells to DsRed positive cells was used to determine the NHEJ or HR activities.

Neutral comet assay

DSBs were analyzed by using the Trevigen Comet Assay Kit (Trevigen, Gaithersburg, MD). HeLa cells were exposed to 8 Gy of X-ray (160 kV, 1.15Gy/min) irradiation by a biological research irradiator (Rad Source Technologies, Suwanee, GA) and cultured for 12 hours. Next, 10 μl trypsinized cells were added to 100 μl molten LMA agarose, then immediately spread onto a CometSlide. The slides were placed at 4°C for 10 min in the dark and subsequently immersed in cold lysis solution for 30 min. The slides were then transferred to a horizontal electrophoresis chamber. Electrophoresis at 20 V for 25 min was performed. The slides were immersed in 70% ethanol for 5 min and stained with SYBR Gold. Images were captured by fluorescence microscope (Leica, Wetzlar, Germany) and analyzed using CaspLab software (30).

Clonogenic survival assay

HeLa cells were plated in triplicate into six-well plate and subjected to various doses of X-ray. Cells were further cultured for 14 days, and then fixed with methanol and stained with 1% crystal violet. Colonies consisting of more than 50 cells were counted as a single colony.

Immunofluorescence

HeLa cells were treated with 8 Gy of X-ray and cultured for 12 hours. Then, cells were fixed with 4% paraformaldehyde in the presence of 0.2% Triton X-100 for 20 min. Then cells were immunostained with antibody against phosphorylated histone H2A variant (γ-H2AX) (Abcam, Cambridge, MA) or p53 binding protein 1 (53BP1) (Novus Biologicals, Littleton, CO).

Western blotting

Cell lysate containing equal amount of protein were subjected to SDS-PAGE, and electrically transferred to PVDF membranes. Nonspecific binding was blocked with Tris-buffered saline containing 5% (w/v) bovine serum albumin. The membranes were incubated with primary antibody for phosphorylated DNA-PKcs (S2056), DNA-PKcs, phosphorylated ATM (S1981), ATM, phosphorylated checkpoint kinase 2 (Chk2), Chk2 (Abcam) and β-actin (Santa Cruz Biochemicals, Santa Cruz, CA) and then incubated with horseradish peroxidase-conjugated second antibody. β-actin was used as a loading control. Immunoblotting signals were detected using an enhanced chemiluminescence method.

Statistical analysis

Data were expressed as mean ± standard deviation. Analysis was performed by Student's t-test or one-way ANOVA following multiple comparisons using SPSS 18.0 software (SPSS Inc., Chicago, IL). Results with a p value less than 0.05 were considered statistically significant.

Results

Quantification of CRISPR/Cas9-induced mutation by HRM analysis

HPRT is located on the X chromosome and has been intensively investigated as a surrogate marker of somatic mutations (31), meanwhile it is also a well-defined candidate gene for targeted genome editing (23,32-34). Here we first constructed a CRISPR/Cas9 plasmid containing the sgRNA sequence targeting the exon 2 of HPRT gene (Fig. 1A). After transfection of the plasmid into HEK293T cells, disruption of the HPRT gene could be validated by the overlapping peaks in the Sanger sequencing data, suggesting the error-prone NHEJ repair of the target site. In order to monitor the time-dependent manner of the Cas9 nuclease-induced mutation, genomic DNA was extracted at different time points after the CRISPR/Cas9 plasmid transfection. A length of 402 bp DNA sequence covering the targeted locus was amplified and subjected to T7E1 assay, which could digest the mismatched heteroduplex formed by the hybridization of the wild-type and mutant HPRT gene and generate two smaller fragments (approximate 130 bp and 270 bp). As shown in Fig. 1B, the mutation frequency reached peak levels at 24 hours post transfection and decreased thereafter, which might due to the proliferation of the cells harbouring a wild-type HPRT. Herein the genomic DNA was collected 24 hours after transfection in the following assay.

Though T7E1 assay could estimate the targeted mutation efficiency (24), analysis of a large amount of samples by PCR, enzymatic digestion and electrophoresis is time-consuming. HRM analysis is an efficient technology for large-scale sequence variant screening by measuring the changes of the T_m of the real-time PCR-amplified fragments. We obtained HRM data from the 157 bp amplicon containing the sgHPRT-targeted site, and the melting curves were converted into a subtractive difference plot to show the fluorescence difference to the references (control plasmid-transfected cells). As shown in Fig. 1C, HRM analysis clearly revealed the disparity of the melting curve between sgHPRT-treated cells and the control group. Parallel experiments, targeting HBEGF locus, were also performed,

and the results of HRM analysis showed the same pattern as that of sgHPRT (Fig. S1). In addition, the flexibility and validity of this mutation exploring approach were confirmed by using T98G and HeLa cells (Fig. S2).

To further examine the robustness of HRM analysis as a quantitative approach, a range of sgHPRT plasmid (from 0 to 8 μg) were mixed with control plasmid to provide a total of 8 μg per aliquot and transfected into HEK293T cells (70% cell confluent in a 60-mm diameter culture dish). It was assumed that transfection of more sgHPRT plasmid could create more DSBs, thus lead to higher mutation efficiency at the targeted site via NHEJ repair. Fig. 1D showed the gradual shift of the subtractive fluorescence difference (ΔF) corresponding to the mutation efficiencies induced by different proportions of CRISPR/Cas9 plasmids. Importantly, the logarithm of ΔF_{max} and the mutation efficiency displayed a strong positive linear correlation (Fig. 1E). These results indicate the usefulness of HRM analysis as a quantitative means to determine the CRISPR/Cas9 plasmid-induced mutation.

Establishment of a screening for NHEJ inhibitors

When different cell lines were transfected with different CRISPR/Cas9 plasmids, different values of ΔF_{max} were obtained (Fig. 1C, S1B, S2A, S2B and S2C). This phenomenon appeared to be related to the variation of the transfection efficiency and chromatin accessibility of sgRNA and Cas9 nuclease at the targeted site, as well as the intrinsic capacity of HRM analysis to resolve the mutation frequency of a given PCR amplicon. An elevated ΔF_{max} value might improve the sensitivity and resolution of the assay. Therefore, the screening was performed using the sgHPRT plasmid and HEK293T cells, by which the highest ΔF_{max} value could be achieved (Fig. 1C and S2C).

The experimental procedures of screening for NHEJ inhibitors were optimized and depicted in Fig. 2A. Five hours after the transfection of sgHPRT plasmid, HEK293T cells were subcultured into 96-well plates at a density of 2×10^4 cells per well. Simultaneously, pharmaceutical compounds were added into the individual wells of the 96-well plates, and incubated for 24 hours. Then genomic DNA was

extracted by a rapid Chelex 100-based method, and targeted locus was amplified and subjected to HRM analysis.

To confirm the feasibility of the screening workflow, we executed the experimental protocols using two DNA-PKcs inhibitors, NU7441 and KU-0060648, which have suppressive effects on NHEJ repair (35,36). As shown in Fig. 2B and 2D, both of the two DNA-PKcs inhibitors declined the ΔF_{max} value in a concentration-dependent manner, implying the reduction of NHEJ-mediated mutations. A significant correlation between the concentrations and the logarithm of ΔF_{max} values were observed (Fig. 2C and 2E). The coefficients of determination R^2 were 0.987 and 0.961 for NU7441 and KU-0060648 respectively. Taken together, these results suggest our screening approach is capable to identify NHEJ inhibitors.

Screening of an approved drug library for NHEJ inhibitors

We performed a screening of an approved drug library including 1540 compounds for NHEJ inhibitors. According to the pharmacological actions, the compounds in the library can be divided into 10 different categories. Multiple colors and numbers (Category No. 1 to 10) were assigned to different categories and the composition of the drug library were demonstrated in a circle chart (Fig. 3A). In order to monitor the screening quality, each screening plate contained control plasmid-transfected cells as references, while sgHPRT plasmid-transfected cells treated with 1% DMSO or 2 μM NU7441 were regarded as negative and positive controls respectively. The final concentration of the screening compounds is 5 μM. The range of Z' factor value was 0.498 - 0.860 (mean value 0.645, 95% confidence interval 0.592 – 0.699), suggesting the excellent screening quality. A full list of the screening results of ΔF_{max} was showed in Table S1, and the sorted data was graphically plotted in Fig. 3B.

Intriguingly, compounds from different categories showed dissimilar distribution of ΔF_{max} values, implying certain pharmacological mechanisms probably underlie the NHEJ inhibitory capacity. Category No. 5 (antineoplastic agents) had the most NHEJ-inhibiting drugs (Fig. S3B), since most of them were known as

DNA-damaging chemicals which could inhibit DNA biosynthesis, or prevent the DNA double helix from being resealed, and thereby impede the NHEJ repair of the HPRT locus (37,38). Remarkably, four cardiac glycosides from Category No. 7 (cardiovascular system) greatly reduced the ΔF_{max} values, that were digtoxin, digoxin, lanatoside C and ouabain (Fig. 3C). In addition, ΔF_{max} values were decreased by a considerable number of compounds from Category No. 8 (nervous system), most of which were neuroleptics and antidepressants (Fig. 3D). Some potential NHEJ inhibitors from other categories were also listed in Fig. S3A, S3C, S3D and S3E. Concerning the potency of the NHEJ-inhibiting effects, we next focused on cardiac glycosides and compounds from Category No. 8 in the following validating investigation.

Screening hits validation

To affirm the screening results, sgHPRT plasmid-transfected HEK293T cells were incubated with different concentration of the screening hits and HRM analysis were repeated, meanwhile cytotoxic effects of these compounds were evaluated by CCK-8 cell viability assay. We identified ouabain and penfluridol as effective NHEJ inhibitors, which could significantly decrease ΔF_{max} values under the non-cytotoxic concentrations (Fig. 4A, 4B and J. Du, unpublished observations), which were 0.1 μM for ouabain and 5 μM for penfluridol.

Next, the effects of ouabain and penfluridol on NHEJ or HR activities were further verified by using engineered GFP gene-based plasmids (28,29). The GFP gene in the NHEJ or HR reporter plasmid is inactivated by an additional exon or by mutations. And recognition sites for a rare-cutting I-SceI endonuclease are inserted into the GFP gene for the induction of DSBs. After digested with I-SceI, the linearized plasmids were transfected into HEK293T cells together with a DsRed plasmid for normalizing transfection efficiency. Successful repair of the I-SceI-induced DSBs by NHEJ or HR could recover the functional GFP gene. As shown in Fig. 4C, NU7441 inhibited NHEJ repair and shifted the balance of DSB

repair towards HR. Both NHEJ and HR activities were suppressed by ouabain treatment, and only NHEJ seemed to be affected by penfluridol treatment.

Evaluation of ouabain and penfluridol as radiosensitizers

The suppressive effects on NHEJ repair of ouabain and penfluridol were merely verified at the CRISPR/Cas9 plasmid target site and the extrachromosomal I-SceI recognition sites. Next, we sought to determine whether these compounds could block the NHEJ repair of the IR-induced DSBs. HeLa cells were pretreated with 0.1 μM ouabain or 5 μM penfluridol for 2 hours, then cells were exposed to 8 Gy of X-ray, and the compounds were further incubated with the cells for 3 hours. Neutral comet assay was performed 12 hours postirradiation to measure the unrepaired DNA fragments. As shown in Fig. 5A, the nuclei of control cells displayed a spherical morphology, indicating the IR-induced DSBs were restored successfully. On the other hand, in the presence of ouabain or penfluridol, the amount of broken DNA was significantly increased, evidenced by the elevated DNA content in the comet tails (Fig. 5A and 5B). Consistently, colony formation assay distinctly showed the radiosensitizing effects of ouabain and penfluridol (Fig. 5C, 5D, 5E and 5F). Collectively, the NHEJ inhibitors revealed by our screening method could impair IR-induced DNA damage repair, hence aggravate the cytotoxicity of IR.

Inhibition of DSB repair by ouabain and penfluridol

Finally, we assessed the nuclear γ-H2AX and 53BP1 foci formations, both of which were the markers of DSBs. HeLa cells were treated with X-ray and NHEJ inhibitors as that of the neutral comet assay. As shown in Fig. 6A, the γ-H2AX and 53BP1 foci of ouabain or penfluridol-treated cells failed to resolve after 12 hours postirradiation compared to the control cells. Western blotting analysis further revealed that ouabain or penfluridol treatment significantly restrained the expression of phosphorylated DNA-PKcs induced by IR (Fig. 6B). However, these NHEJ inhibitors did not seem to interact directly with DNA-PKcs, since they failed to show

any inhibitory effects on DNA-PK kinase activity in vitro (Fig. S4). Moreover, they might not suppress the activation of ATM in response to IR, as well as its downstream target, Chk2. These data suggest that ouabain and penfluridol might interrupt DSB repair by preventing DNA-PKcs from being activated.

Discussion

Highlighting the essential role of the NHEJ pathway to resolve highly cytotoxic DSBs, identification of novel NHEJ inhibitors holds great promise for augmenting cancer therapeutic efficiency of genotoxic treatment (2,3). Here, we designed and carried out an NHEJ inhibitor screening, which mainly involved the following two steps: first create a genomic specific DSB by CRISPR/Cas9 system, second evaluate the mutation frequencies of the targeted site by HRM analysis. Our results affirmed a positive correlation between NHEJ activities and mutation frequencies of the targeted site. By means of this approach, several hits were emerged as novel NHEJ inhibitors. The most noteworthy result was the inhibition of NHEJ by cardiac glycosides and a number of compounds affecting neurotransmitters. Further examination revealed ouabain and penfluridol had the suppressive effects on IR-induced DSB repair, thus increased the radiosensitivity of HeLa cells. Preliminary evidences indicated the inhibitory effects of these compounds on the DNA-PKcs phosphorylation induced by IR exposure.

Owing to the complexity of HR and NHEJ pathway, several cell-based systems have been developed to screening the novel DSB repair inhibitors. In these approaches, DSBs were mainly introduced by IR or rare cutting meganuclease I-SceI (39-42), and the consequences of DSB repair were deduced by the results of neutral single-cell electrophoresis (39), colony formation assay (40), expressions of DSB repair-dependent fluorescent protein (41) or fluorescent staining of HR and NHEJ specific foci (42). Because NHEJ is the predominant DSB repair pathway, there is rationale in monitoring its activity to facilitate the screening of radiosensitizers. Theoretically, higher mutation frequencies at the DSB sites correlate the higher levels of NHEJ activities. But it is unachievable to locate the NHEJ-mediated mutational sites in the genome because of the stochastic DSBs induced by IR.

By virtue of the exquisite specificity of Cas9-induced DSBs, the repair consequences of the targeted loci can be analyzed directly and quantitatively. For example, a sequence trace decomposition strategy has been developed for the

identification of short sequence deletions and insertions (43), and it has been reported that a digital PCR-based assay enabled the simultaneous detection of HR and NHEJ of the nuclease-induced DSBs (44). It is not surprising that both of these approaches generally relied on PCR amplification of the targeted sequences. We also used a PCR-based method termed HRM analysis, which involves only about 30 min of automatic fluorescence acquisition after the PCR reaction in the presence of a suitable saturating dye (21,22). And mutation frequencies assessed by subtractive transformation of the melting fluorescent data could distinguish the altered levels of NHEJ activities. Treatment of NU7441 and KU-0060648, known to block NHEJ repair via DNA-PKcs inhibition, exhibited a dose-dependent reduction of the mutation frequencies, reflecting by the ΔF_{max} values. This suggest that NHEJ inhibitory capacity could be deciphered by ΔF_{max} assessment. This rapid and closed-tube technique enabled the screening of a large number of samples for NHEJ inhibitors. Though we employed only HEK293T cells for the screening study, this approach can be applied to other cell lines, such as the tumor cells with a given genetic background, therefore, the cell type-specific NHEJ inhibitors or novel NHEJ mechanisms might be disclosed.

A limitation of our screening assay is that the status of HR repair remains elusive. Since HR repair preserves the genomic integrity, HRM analysis is unable to detect the unaltered sequence information. Indeed, Cas9-induced DSBs have an eventual tendency towards NHEJ repair, because if a given DSB is repaired by HR, the locus will be continuously recut by Cas9 nuclease until the protospacer adjacent motif or sgRNA binding sequences are disrupted through NHEJ repair (45). HR repair directed by a third donor template may prevent the cycles of cleavage and ligation, however, the donor template is extrachromosomal and dominant in quantity, whereas the endogenous template for HR repair is only on the equivalent position of the sister chromatid during the S and G2 phases, hence the HR activity is difficult to estimate in the normal context of chromatin. By using a GFP-based plasmid religation assay, ouabain, but not penfluridol, showed an inhibitory effect on HR activities, suggesting

that the NHEJ inhibitors revealed by our screening assay might also affect HR repair through frustrating the upstream signaling events responsible for both NHEJ and HR.

In order to better understand the NHEJ inhibitory capacity of the screening drugs, the data were generally classified by their pharmacological activities. Consistent with a previous screening study (42), our results suggest that cardiac glycosides might serve as promising DSB repair inhibitors. Cardiac glycosides are well-established Na^+/K^+-ATPase inhibitors and have been widely used in the treatment of congestive heart failure and atrial arrhythmia for a long time (46). Most notably, numerous reports have suggested that cancer cells are susceptible to cardiac glycosides and several derivatives have entered clinical trials either as monotherapy or combined with conventional regimens (47-50). It has been also uncovered that cardiac glycosides impaired DNA damage repair and diminish radioresistance of cancer cells (51-54). Given the relative low cytotoxicity, ouabain might be therapeutically favourable radiosensitizer, and the effects of ouabain should be further investigated in xenograft models. Though the detailed molecular mechanisms of cardiac glycoside-induced radiosensitization have not been fully understood, our results suggest that ouabain could prevent DNA-PKcs activation, thus inhibit NHEJ activities.

Another kind of NHEJ inhibitors revealed by the screening were the drugs for the treatment of psychiatric disorders. Among them, penfluridol appeared to be a potential candidate for radiosensitization. Interestingly, besides the NHEJ inhibitory effects displayed by our results, multiple mechanisms of anti-tumor function of penfluridol have been reported, including production of reactive oxygen species, suppression of metastasis and induction of autophagy-mediated apoptosis (55-57). In addition, trifluoperazine, a member of the phenothiazines sharing the inhibitory activity against dopamine D2 receptor with penfluridol, has NHEJ-suppressive capacity via DNA-PK inhibition (58,59). This strongly suggests that antipsychotics could be readily repurposed as radiosensitizers.

In conclusion, CRISPR/Cas9 system, the highly efficient and versatile tool for genome editing, functioned as a pair of precise scissors in the screening assay. Then

the DNA breakage was sewn together by the error-prone NHEJ. Finally, HRM analysis, the quality inspector, rigidly discriminated the patchy DNA. Through screening an approved drug library, several drugs were identified as potential NHEJ inhibitors, and the radiosensitizing effects of ouabain and penfluridol were clearly demonstrated in vitro. Despite the fact that the molecular mechanisms exquisitely governing NHEJ repair have not been completely elucidated, the robust and flexible CRISPR/Cas9-based NHEJ inhibitor screening strategy might pave the way for exploring novel radiosensitizers. Mechanistic investigation of the new NHEJ inhibitors will provide new insights into how cell orchestrate the DNA damage response and allow the identification of vulnerable targets for cancer therapy. Importantly, it is necessary to put more efforts to optimize the inhibitory specificity against NHEJ and minimize the undesirable pharmacological actions. Detailed exploration of the activities of the NHEJ inhibitor analogs and derivatives might represent a feasible solution for successful translation of these inhibitors into clinical applications.

Acknowledgements

We would like to thank Dr. Vera Gorbunova (University of Rochester) and Dr. Mao Zhiyong (Tongji University) for kindly providing the NHEJ and HR reporter plasmid. We acknowledge the Priority Academic Program Development of Jiangsu Higher Education Institutions (PAPD).

References

1. Lord CJ, Ashworth A. The DNA damage response and cancer therapy. Nature 2012;481:287-94.
2. O'Connor MJ. Targeting the DNA damage response in cancer. Mol Cell 2015;60:547-60.
3. Pearl LH, Schierz AC, Ward SE, Al-Lazikani B, Pearl FM. Therapeutic opportunities within the DNA damage response. Nat Rev Cancer 2015;15:166-80.
4. Vilenchik MM, Knudson AG. Endogenous DNA double-strand breaks: production, fidelity of repair, and induction of cancer. Proc Natl Acad Sci U S A 2003;100:12871-6.
5. Rothkamm K, Barnard S, Moquet J, Ellender M, Rana Z, Burdak-Rothkamm S. DNA damage foci: meaning and significance. Environ Mol Mutagen 2015;56:491-504.
6. Bennett CB, Lewis AL, Baldwin KK, Resnick MA. Lethality induced by a single site-specific double-strand break in a dispensable yeast plasmid. Proc Natl Acad Sci U S A 1993;90:5613-7.
7. Jackson SP, Bartek J. The DNA-damage response in human biology and disease. Nature 2009;461:1071-8.
8. Ceccaldi R, Rondinelli B, D'Andrea AD. Repair pathway choices and consequences at the double-strand break. Trends Cell Biol 2016;26:52-64.
9. Beucher A, Birraux J, Tchouandong L, Barton O, Shibata A, Conrad S, et al. ATM and Artemis promote homologous recombination of radiation-induced DNA double-strand breaks in G2. EMBO J 2009;28:3413-27.
10. Shibata A, Conrad S, Birraux J, Geuting V, Barton O, Ismail A, et al. Factors determining DNA double-strand break repair pathway choice in G2 phase. EMBO J 2011;30:1079-92.

11. Karanam K, Kafri R, Loewer A, Lahav G. Quantitative live cell imaging reveals a gradual shift between DNA repair mechanisms and a maximal use of HR in mid S phase. Mol Cell 2012;47:320-9.
12. Curtin NJ. Inhibiting the DNA damage response as a therapeutic manoeuvre in cancer. Br J Pharmacol 2013;169:1745-65.
13. Leahy JJ, Golding BT, Griffin RJ, Hardcastle IR, Richardson C, Rigoreau L, et al. Identification of a highly potent and selective DNA-dependent protein kinase (DNA-PK) inhibitor (NU7441) by screening of chromenone libraries. Bioorg Med Chem Lett 2004;14:6083-7.
14. Mortensen DS, Perrin-Ninkovic SM, Shevlin G, Elsner J, Zhao J, Whitefield B, et al. Optimization of a series of triazole containing mammalian target of rapamycin (mTOR) kinase inhibitors and the discovery of CC-115. J Med Chem 2015;58:5599-608.
15. Hickson I, Zhao Y, Richardson CJ, Green SJ, Martin NM, Orr AI, et al. Identification and characterization of a novel and specific inhibitor of the ataxia-telangiectasia mutated kinase ATM. Cancer Res 2004;64:9152-9.
16. Rainey MD, Charlton ME, Stanton RV, Kastan MB. Transient inhibition of ATM kinase is sufficient to enhance cellular sensitivity to ionizing radiation. Cancer Res 2008;68:7466-74.
17. Liu JF, Konstantinopoulos PA, Matulonis UA. PARP inhibitors in ovarian cancer: current status and future promise. Gynecol Oncol 2014;133:362-9.
18. Nile DL, Rae C, Hyndman IJ, Gaze MN, Mairs RJ. An evaluation in vitro of PARP-1 inhibitors, rucaparib and olaparib, as radiosensitisers for the treatment of neuroblastoma. BMC Cancer 2016;16:621.
19. Doudna JA, Charpentier E. Genome editing. The new frontier of genome engineering with CRISPR-Cas9. Science 2014;346:1258096.
20. Hsu PD, Lander ES, Zhang F. Development and applications of CRISPR-Cas9 for genome engineering. Cell 2014;157:1262-78.
21. Taylor CF. Mutation scanning using high-resolution melting. Biochem Soc Trans 2009;37:433-7.

22. Vossen RH, Aten E, Roos A, den Dunnen JT. High-resolution melting analysis (HRMA): more than just sequence variant screening. Hum Mutat 2009;30:860-6.
23. Smurnyy Y, Cai M, Wu H, McWhinnie E, Tallarico JA, Yang Y, et al. DNA sequencing and CRISPR-Cas9 gene editing for target validation in mammalian cells. Nat Chem Biol 2014;10:623-5.
24. Zhou Y, Zhu S, Cai C, Yuan P, Li C, Huang Y, et al. High-throughput screening of a CRISPR/Cas9 library for functional genomics in human cells. Nature 2014;509:487-91.
25. Wittwer CT, Reed GH, Gundry CN, Vandersteen JG, Pryor RJ. High-resolution genotyping by amplicon melting analysis using LCGreen. Clin Chem 2003;49:853-60.
26. Palais R, Wittwer CT. Mathematical algorithms for high-resolution DNA melting analysis. Methods Enzymol 2009;454:323-43.
27. Zhang JH, Chung TD, Oldenburg KR. A simple statistical parameter for use in evaluation and validation of high throughput screening assays. J Biomol Screening 1999;4:67-73.
28. Mao Z, Hine C, Tian X, Van Meter M, Au M, Vaidya A, et al. SIRT6 promotes DNA repair under stress by activating PARP1. Science 2011;332:1443-6.
29. Li Z, Zhang W, Chen Y, Guo W, Zhang J, Tang H, et al. Impaired DNA double-strand break repair contributes to the age-associated rise of genomic instability in humans. Cell Death Differ 2016;23:1765-77.
30. Konca K, Lankoff A, Banasik A, Lisowska H, Kuszewski T, Gozdz S, et al. A cross-platform public domain PC image-analysis program for the comet assay. Mutat Res 2003;534:15-20.
31. Albertini RJ. HPRT mutations in humans: biomarkers for mechanistic studies. Mutat Res 2001;489:1-16.
32. Gravells P, Ahrabi S, Vangala RK, Tomita K, Brash JT, Brustle LA, et al. Use of the HPRT gene to study nuclease-induced DNA double-strand break repair. Hum Mol Genet 2015;24:7097-110.

33. He Z, Proudfoot C, Mileham AJ, McLaren DG, Whitelaw CB, Lillico SG. Highly efficient targeted chromosome deletions using CRISPR/Cas9. Biotechnol Bioeng 2015;112:1060-4.
34. Liao S, Tammaro M, Yan H. Enriching CRISPR-Cas9 targeted cells by co-targeting the HPRT gene. Nucleic Acids Res 2015;43:e134.
35. Zhao Y, Thomas HD, Batey MA, Cowell IG, Richardson CJ, Griffin RJ, et al. Preclinical evaluation of a potent novel DNA-dependent protein kinase inhibitor NU7441. Cancer Res 2006;66:5354-62.
36. Munck JM, Batey MA, Zhao Y, Jenkins H, Richardson CJ, Cano C, et al. Chemosensitization of cancer cells by KU-0060648, a dual inhibitor of DNA-PK and PI-3K. Mol Cancer Ther 2012;11:1789-98.
37. Cheung-Ong K, Giaever G, Nislow C. DNA-damaging agents in cancer chemotherapy: serendipity and chemical biology. Chem Biol 2013;20:648-59.
38. Gavande NS, VanderVere-Carozza PS, Hinshaw HD, Jalal SI, Sears CR, Pawelczak KS, et al. DNA repair targeted therapy: The past or future of cancer treatment? Pharmacol Ther 2016;160:65-83.
39. Weingeist DM, Ge J, Wood DK, Mutamba JT, Huang Q, Rowland EA, et al. Single-cell microarray enables high-throughput evaluation of DNA double-strand breaks and DNA repair inhibitors. Cell Cycle 2013;12:907-15.
40. Tiwana GS, Prevo R, Buffa FM, Yu S, Ebner DV, Howarth A, et al. Identification of vitamin B1 metabolism as a tumor-specific radiosensitizing pathway using a high-throughput colony formation screen. Oncotarget 2015;6:5978-89.
41. Goglia AG, Delsite R, Luz AN, Shahbazian D, Salem AF, Sundaram RK, et al. Identification of novel radiosensitizers in a high-throughput, cell-based screen for DSB repair inhibitors. Mol Cancer Ther 2015;14:326-42.
42. Surovtseva YV, Jairam V, Salem AF, Sundaram RK, Bindra RS, Herzon SB. Characterization of cardiac glycoside natural products as potent inhibitors of DNA double-strand break repair by a whole-cell double immunofluorescence assay. J Am Chem Soc 2016;138:3844-55.

43. Brinkman EK, Chen T, Amendola M, van Steensel B. Easy quantitative assessment of genome editing by sequence trace decomposition. Nucleic Acids Res 2014;42:e168.
44. Miyaoka Y, Berman JR, Cooper SB, Mayerl SJ, Chan AH, Zhang B, et al. Systematic quantification of HDR and NHEJ reveals effects of locus, nuclease, and cell type on genome-editing. Sci Rep 2016;6:23549.
45. Paquet D, Kwart D, Chen A, Sproul A, Jacob S, Teo S, et al. Efficient introduction of specific homozygous and heterozygous mutations using CRISPR/Cas9. Nature 2016;533:125-9.
46. Lingrel JB. The physiological significance of the cardiotonic steroid/ouabain-binding site of the Na,K-ATPase. Annu Rev Physiol 2010;72:395-412.
47. Prassas I, Diamandis EP. Novel therapeutic applications of cardiac glycosides. Nat Rev Drug Discovery 2008;7:926-35.
48. Menger L, Vacchelli E, Kepp O, Eggermont A, Tartour E, Zitvogel L, et al. Trial watch: cardiac glycosides and cancer therapy. Oncoimmunology 2013;2:e23082.
49. Slingerland M, Cerella C, Guchelaar HJ, Diederich M, Gelderblom H. Cardiac glycosides in cancer therapy: from preclinical investigations towards clinical trials. Invest New Drugs 2013;31:1087-94.
50. Calderon-Montano JM, Burgos-Moron E, Orta ML, Maldonado-Navas D, Garcia-Dominguez I, Lopez-Lazaro M. Evaluating the cancer therapeutic potential of cardiac glycosides. BioMed Res Int 2014;2014:794930.
51. Nasu S, Milas L, Kawabe S, Raju U, Newman R. Enhancement of radiotherapy by oleandrin is a caspase-3 dependent process. Cancer Lett 2002;185:145-51.
52. Wang L, Raju U, Milas L, Molkentine D, Zhang Z, Yang P, et al. Huachansu, containing cardiac glycosides, enhances radiosensitivity of human lung cancer cells. Anticancer Res 2011;31:2141-8.
53. Jun DW, Hwang M, Kim HJ, Hwang SK, Kim S, Lee CH. Ouabain, a cardiac glycoside, inhibits the Fanconi anemia/BRCA pathway activated by DNA interstrand cross-linking agents. PLoS One 2013;8:e75905.

54. Kang MA, Kim MS, Kim W, Um JH, Shin YJ, Song JY, et al. Lanatoside C suppressed colorectal cancer cell growth by inducing mitochondrial dysfunction and increased radiation sensitivity by impairing DNA damage repair. Oncotarget 2016;7:6074-87.
55. Hedrick E, Li X, Safe S. Penfluridol represses integrin expression in breast cancer through induction of reactive oxygen species and downregulation of Sp transcription factors. Mol Cancer Ther 2017;16:205-16.
56. Ranjan A, Gupta P, Srivastava SK. Penfluridol: An antipsychotic agent suppresses metastatic tumor growth in triple-negative breast cancer by inhibiting integrin signaling axis. Cancer Res 2016;76:877-90.
57. Ranjan A, Srivastava SK. Penfluridol suppresses pancreatic tumor growth by autophagy-mediated apoptosis. Sci Rep 2016;6:26165.
58. Eriksson A, Yachnin J, Lewensohn R, Nilsson A. DNA-dependent protein kinase is inhibited by trifluoperazine. Biochem Biophys Res Commun 2001;283:726-31.
59. Polischouk AG, Holgersson A, Zong D, Stenerlow B, Karlsson HL, Moller L, et al. The antipsychotic drug trifluoperazine inhibits DNA repair and sensitizes non small cell lung carcinoma cells to DNA double-strand break induced cell death. Mol Cancer Ther 2007;6:2303-9.

Figure Legends

Figure 1. Quantitative detection of sgHPRT-induced mutation by HRM analysis. (A) Graphical representation of the targeting of HPRT locus using CRISPR/Cas9 system. (B) HEK293T cells were transfected with sgHPRT plasmid and genomic DNA was extracted at different time points. T7E1 cleavage assay was performed to evaluate the targeted mutation. (C) Melting data were collected and normalized as describle in the Material and Methods (upper panel), and a subtractive plot showed the relative fluorescence difference (ΔF) to the control curve (lower pannel). (D) Different mutation efficiencies were induced by transfection of proportional sgHPRT and control plasmid. The data were presented in a three-dimension plot where X-axis showed the temperature, Y-axis showed the ΔF and Z-axis showed the mutation efficiency. (E) Correlation of the mutation efficiency with the maximum value of ΔF (ΔF_{max}).

Figure 2. Design and validation of the screening for NHEJ inhibitors. (A) Schematic depicting the screening procedures. HEK293T cells were transfected with sgHPRT plasmid for 5 hours, and subcultured into 96-well plates in the present of the screening compounds. Twenty-four hours later, genomic DNA was extracted and subjected to HRM analysis. Two DNA-PKcs inhibitors, NU7441 and KU-0060648, were incubated with cells in the 96-well plates. Three-dimension plots show the HRM data of different concentrations of NU7441 (B) and KU-0060648 (D). Linear correlation between the concentrations and ΔF_{max} for NU7441 (C) and KU-0060648 (E).

Figure 3.

Results of the screening of an approved drug library. (A) The drugs were classified according to their pharmacological action. The composition of the 10 categories was shown in the circle chart. (B) Scatter plots of the screening results of 1540 compounds.

Tables of top hits of Category No. 7 (cardiovascular system) (C) and Category No. 8 (nervous system) (D).

Figure 4.

Dose-response analysis of the screening hits. The chemical structures, and the cytotoxic and NHEJ-inhibiting effects of ouabain (A) and penfluridol (B) were shown in a dose-dependent manner. HEK293T cells were treated with different concentration of ouabain or penfluridol for 24 hours. (C) Measurement of NHEJ and HR activities by using the NHEJ and HR reporter plasmids. HEK293T cells were transfected with I-SceI-linearized plasmids and incubated with ouabain or penfluridol for 24 hours. A DsRed-expressing plasmid was co-transfected as transfection control. Recircularized plasmids by NHEJ or HR have the intact GFP gene which can be assayed by flow cytometry. *, $p < 0.05$; **, $p < 0.01$ vs DMSO-treated group, $n = 4$.

Figure 5.

Radiosensitizing effects of ouabain and penfluridol. (A) HeLa cells were incubated with 0.1 μM ouabain or 5 μM penfluridol for 2 hours, then exposed to 8 Gy of X-ray, and further incubated with these drugs for 3 hours. Neutral comet assay was performed 12 hours postirradiation. (B) The percentage of DNA content in the tails were analyzed. *, $p < 0.05$ vs DMSO-treated group, $n = 3$. Representative images of the colony formation assay of ouabain (C) and penfluridol (E) were shown. Treatment of ouabain (D) and penfluridol (F) increased the radiosensitivity of HeLa cells. *, $p < 0.05$ vs DMSO-treated group, $n = 3$.

Figure 6.

Impairment of DSB repair by ouabain and penfluridol. (A) HeLa cells were incubated with 0.1 μM ouabain or 5 μM penfluridol for 2 hours, then exposed to 8 Gy of X-ray, and further incubated with these drugs for 3 hours. Twelve hours postirradiation, γ-H2AX and 53BP1 foci formations were visualized by immunofluorescent staining.

(B) Four hours postirradiation, the expressions of phosphorylated DNA-PKcs, ATM and Chk2 were analyzed by western blotting. *, $p < 0.05$ vs DMSO-treated group, $n = 3$.

Author Manuscript Published OnlineFirst on September 1, 2017; DOI: 10.1158/1535-7163.MCT-17-0090
Author manuscripts have been peer reviewed and accepted for publication but have not yet been edited.

Figure 1

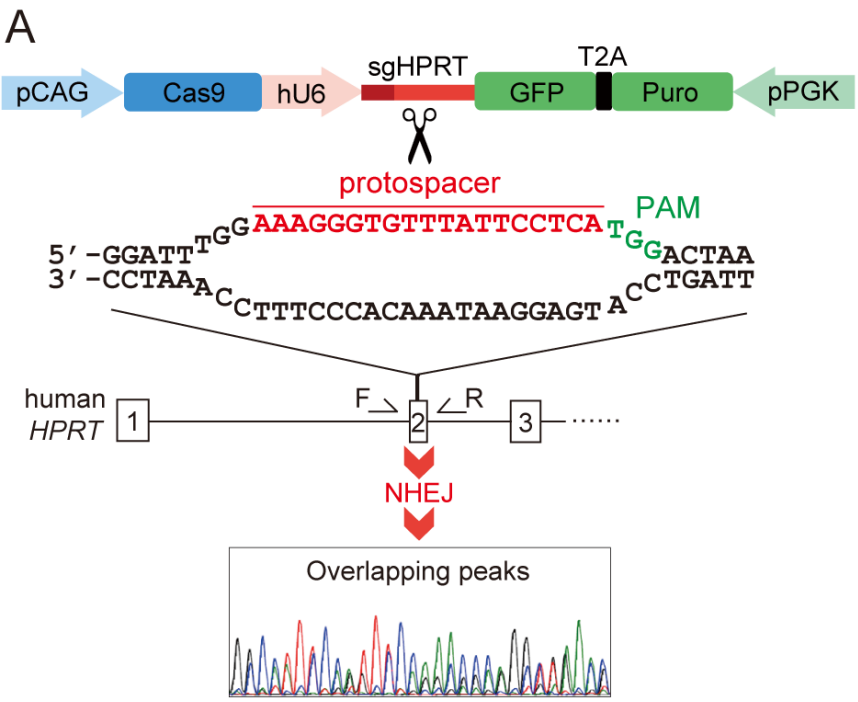

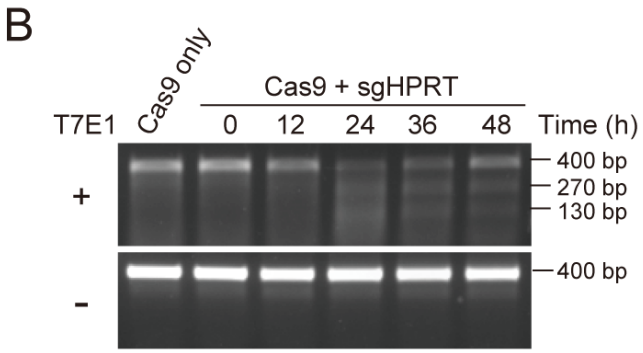

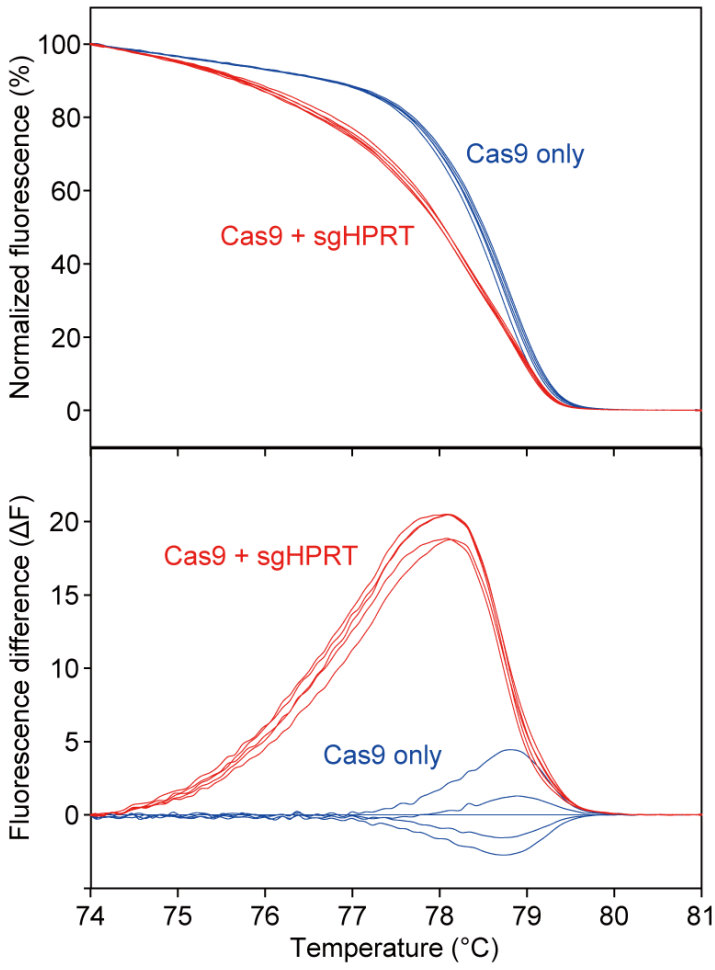

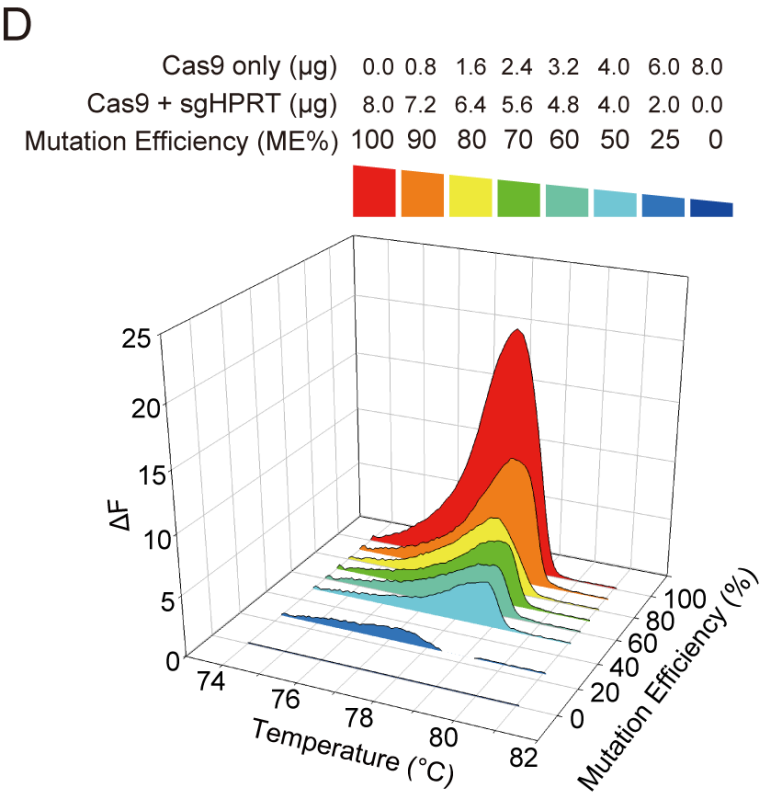

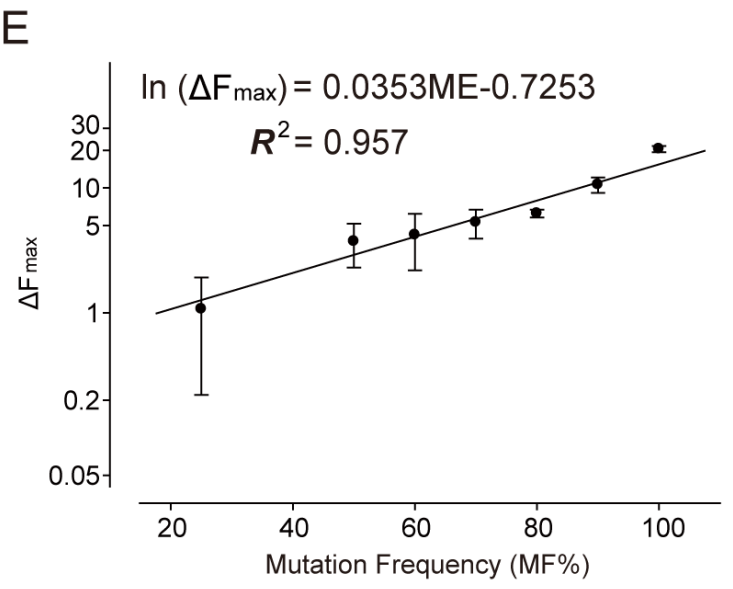

Author Manuscript Published OnlineFirst on September 1, 2017; DOI: 10.1158/1535-7163.MCT-17-0090
Author manuscripts have been peer reviewed and accepted for publication but have not yet been edited.

Figure 2

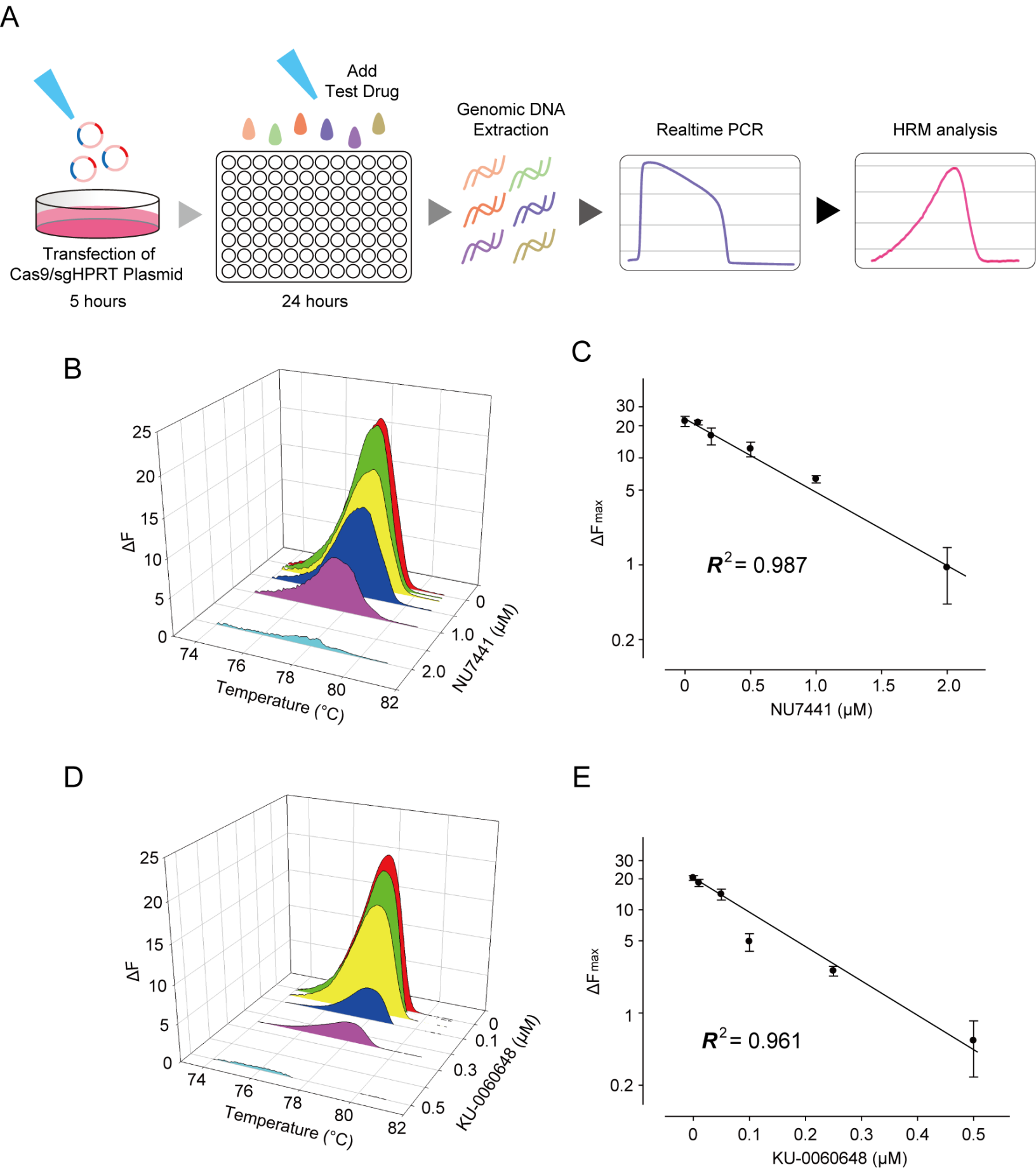

Author Manuscript Published OnlineFirst on September 1, 2017; DOI: 10.1158/1535-7163.MCT-17-0090
Author manuscripts have been peer reviewed and accepted for publication but have not yet been edited.

Figure 3

A

Respiratory system	1	2.66%	(41)
Endocrine system	2	3.25%	(50)
Metabolic system	3	3.83%	(59)
Immune system	4	3.96%	(61)
Antineoplastics	5	6.04%	(93)
Anti-inflammation	6	7.60%	(117)
Cardiovascular system	7	11.82%	(182)
Nervous system	8	16.95%	(261)
Anti-infectives	9	22.73%	(350)
Other	10	21.17%	(326)
Sum		100.00%	(1540)

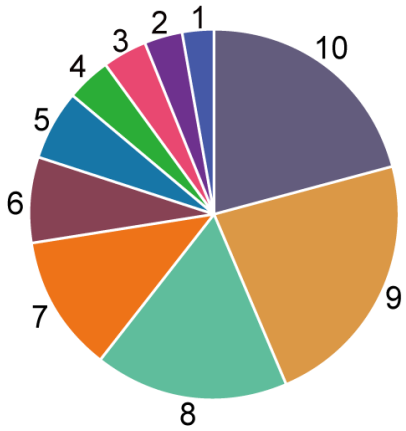

B

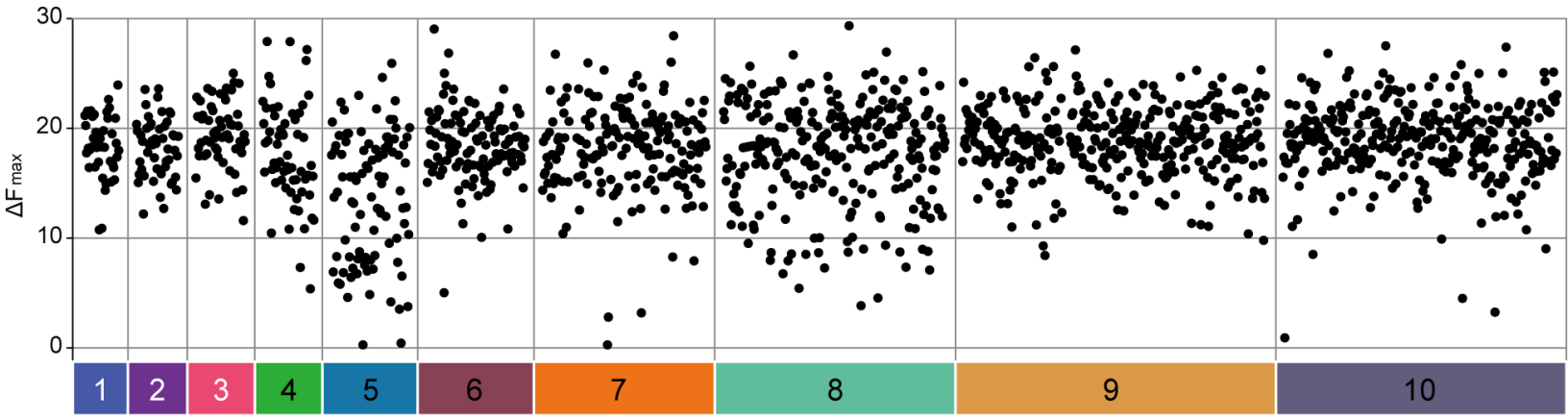

C

7	Drug	CAS No.	Classification	ΔF_{max}
	Digitoxin	71-63-6	Cardiac glycoside	0.19
	Digoxin	20830-75-5	Cardiac glycoside	2.72
	Lanatoside C	17575-22-3	Cardiac glycoside	3.11
	Suloctidil	54767-75-8	Vasoactive antiplatelet drug	7.83
	Ouabain octahydrate	11018-89-6	Cardiac glycoside	8.18

D

8	Drug	CAS No.	Classification	ΔF_{max}
	Penfluridol	26864-56-2	Antipsychotic	4.46
	Doxepin hydrochloride	1229-29-4	Antidepressant	5.34
	Citalopram hydrochloride	59729-32-7	Antidepressant	6.66
	Trazodone hydrochloride	25332-39-2	Antidepressant	7.00
	Iloperidone	133454-47-4	Antipsychotic	7.19
	Risperidal	106266-06-2	Antipsychotic	7.25
	Cytidine 5'-diphosphocholine	987-78-0	Psychostimulant	7.84
	Blonanserin	132810-10-7	Antipsychotic	7.88
	Escitalopram	128196-01-0	Antidepressant	8.42
	Desipramine hydrochloride	58-28-6	Antidepressant	8.46

Author Manuscript Published OnlineFirst on September 1, 2017; DOI: 10.1158/1535-7163.MCT-17-0090
Author manuscripts have been peer reviewed and accepted for publication but have not yet been edited.

Figure 4

A

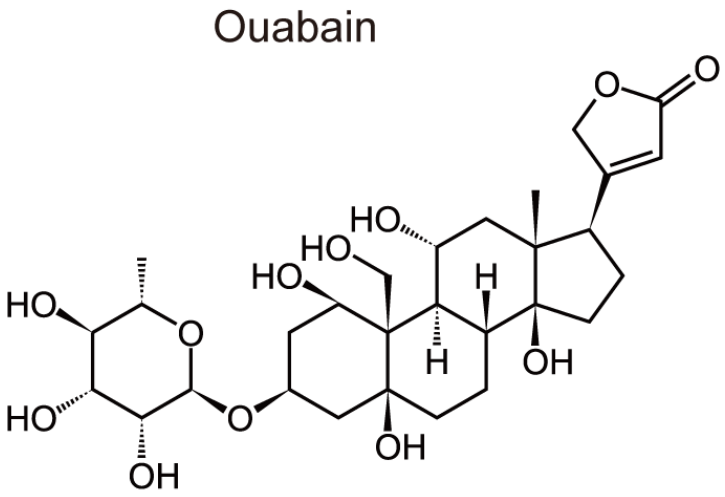

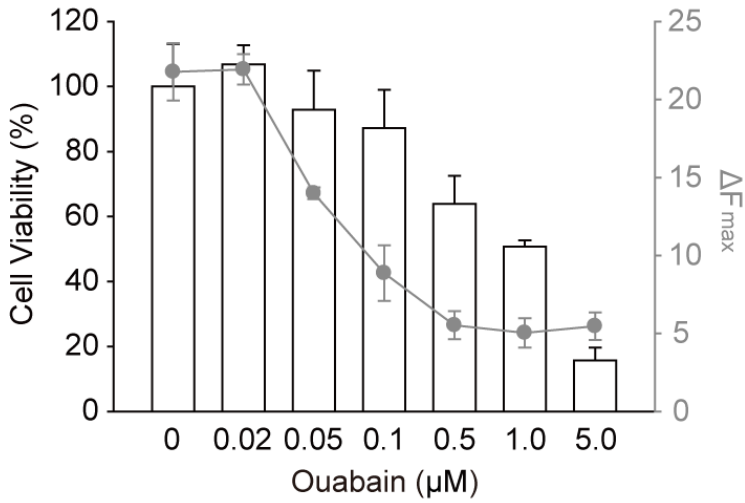

B

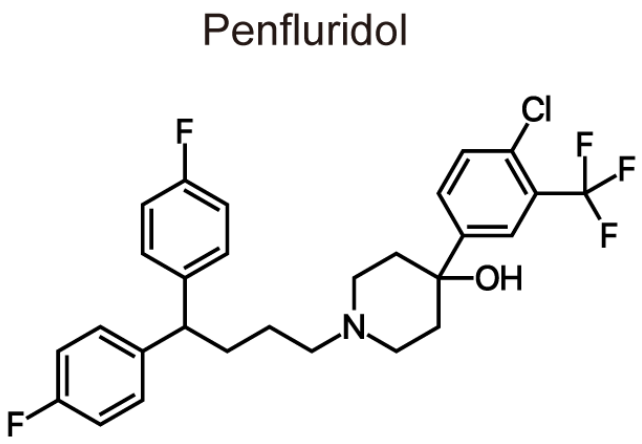

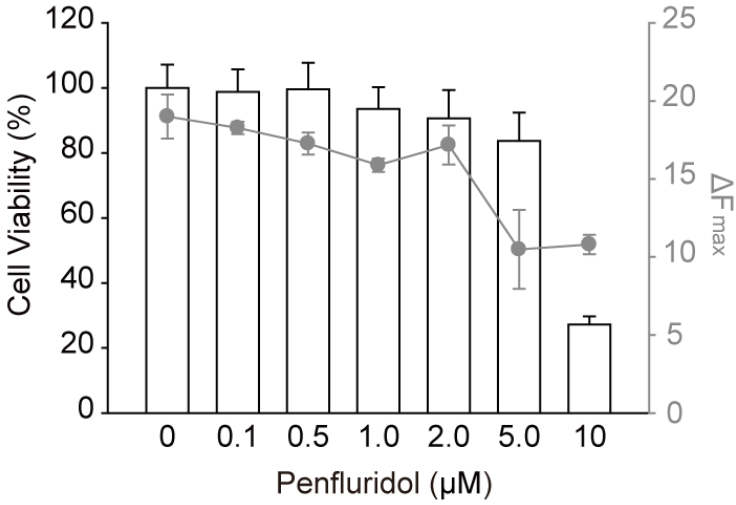

C

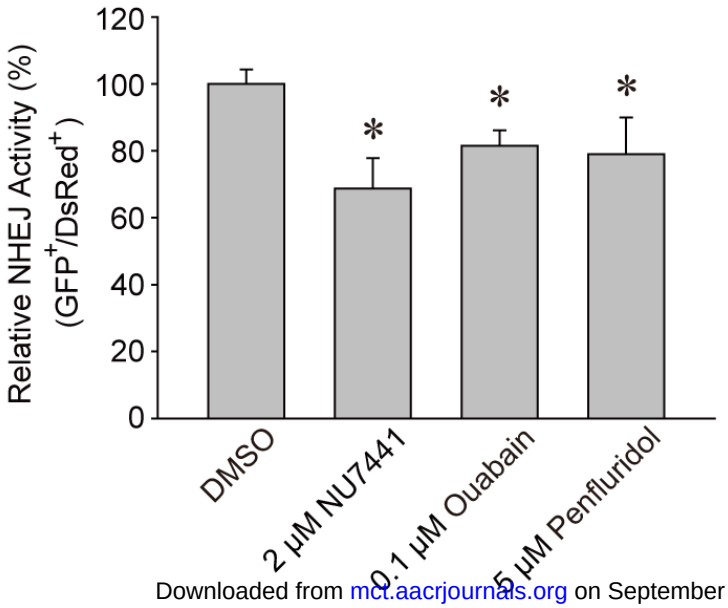

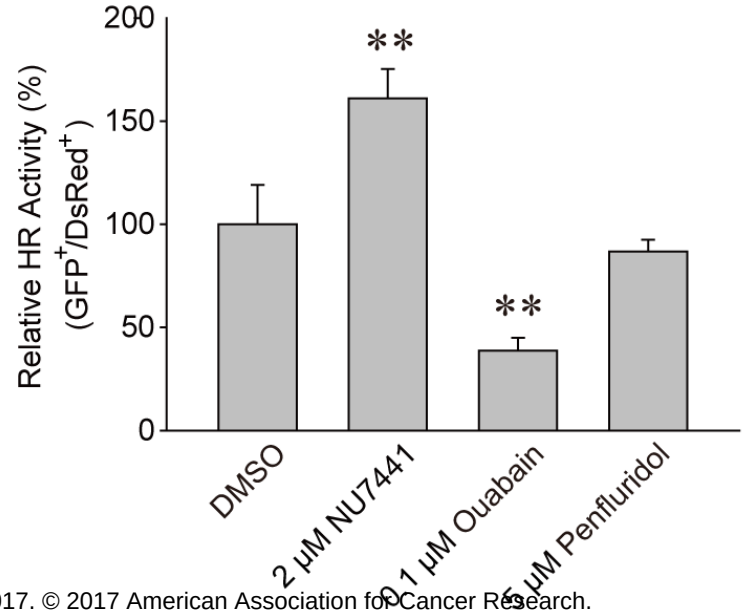

Author Manuscript Published OnlineFirst on September 1, 2017; DOI: 10.1158/1535-7163.MCT-17-0090
Author manuscripts have been peer reviewed and accepted for publication but have not yet been edited.

Figure 5

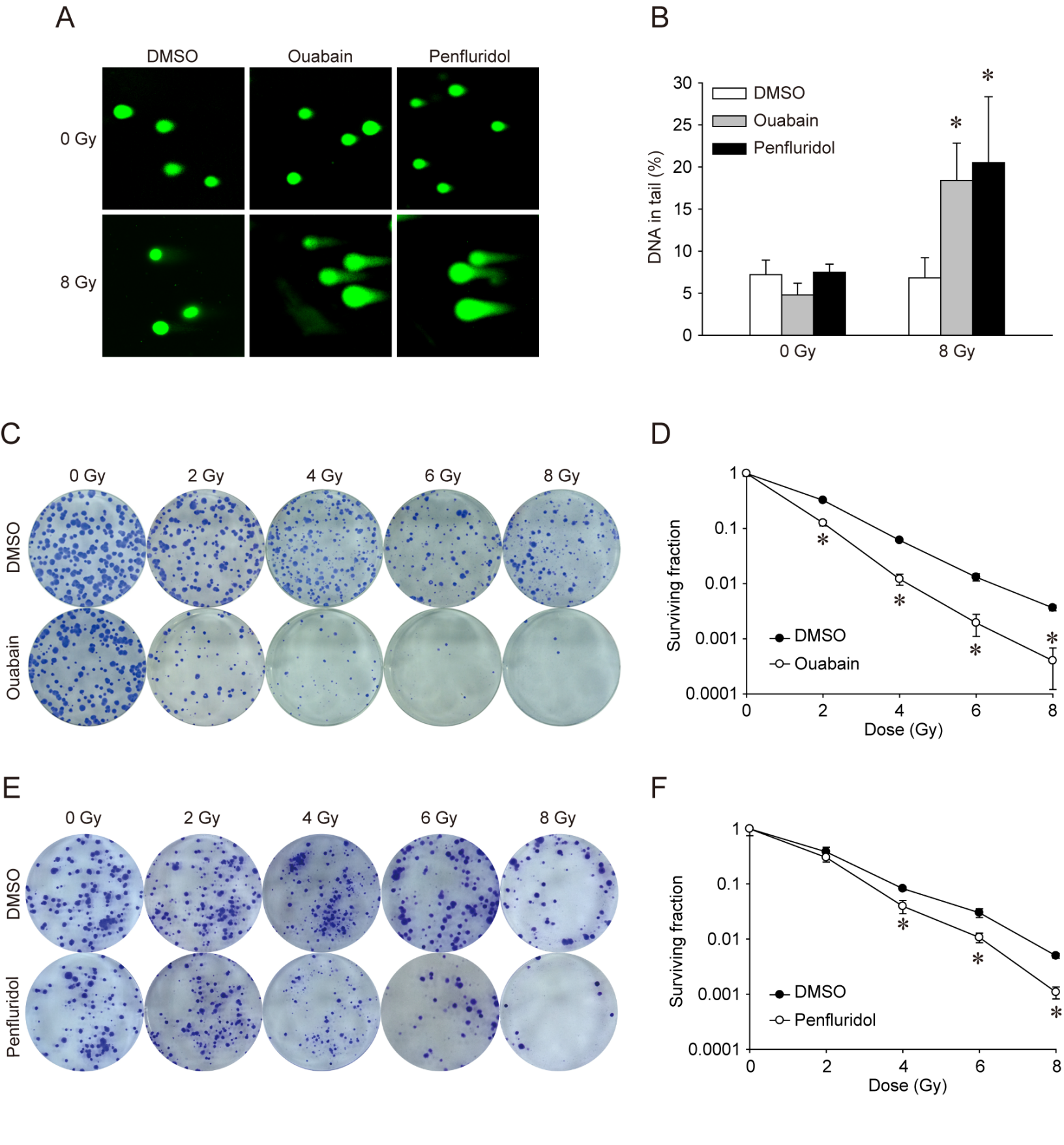

Figure 6

Author Manuscript Published OnlineFirst on September 1, 2017; DOI: 10.1158/1535-7163.MCT-17-0090
Author manuscripts have been peer reviewed and accepted for publication but have not yet been edited.

A

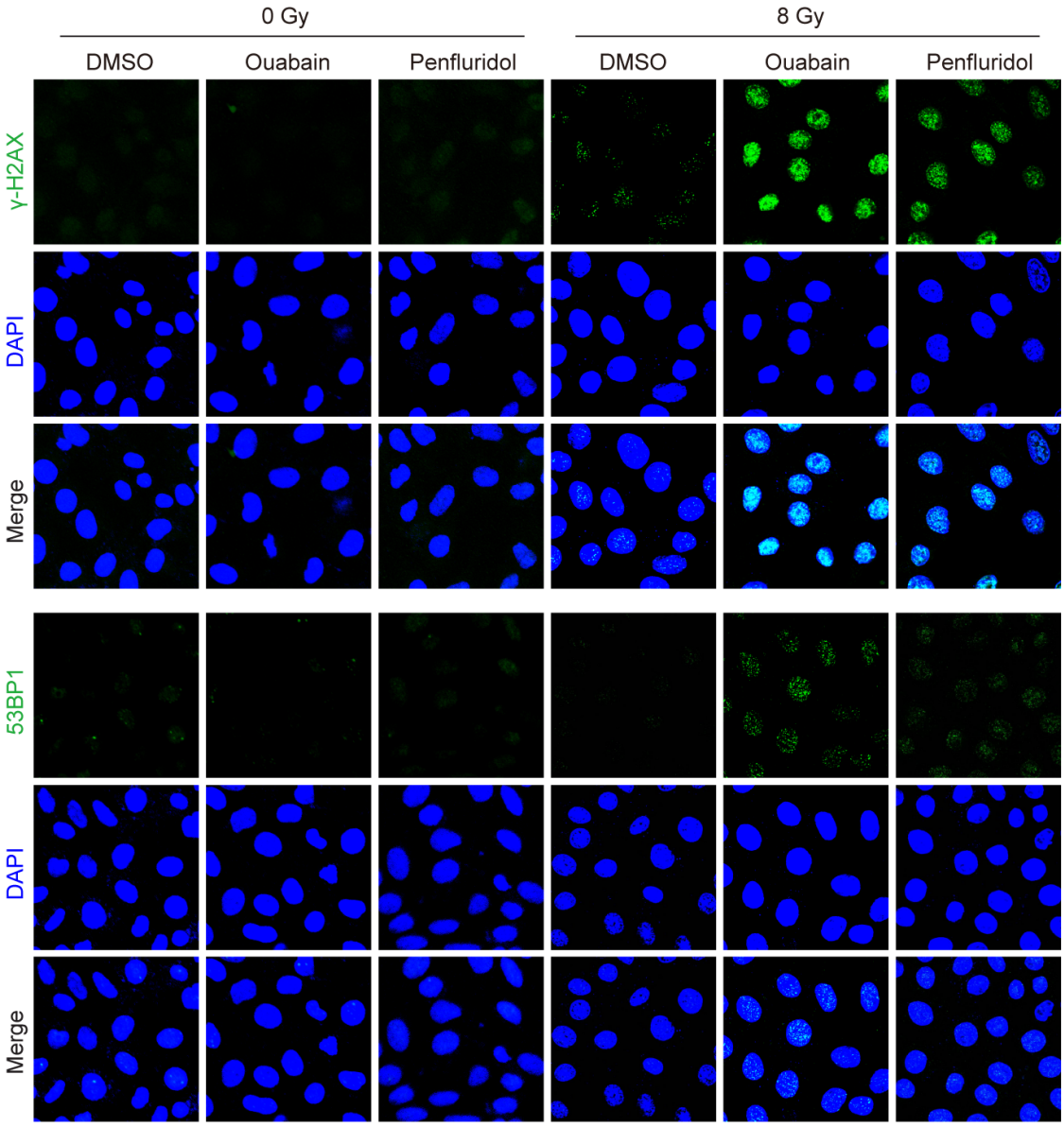

B

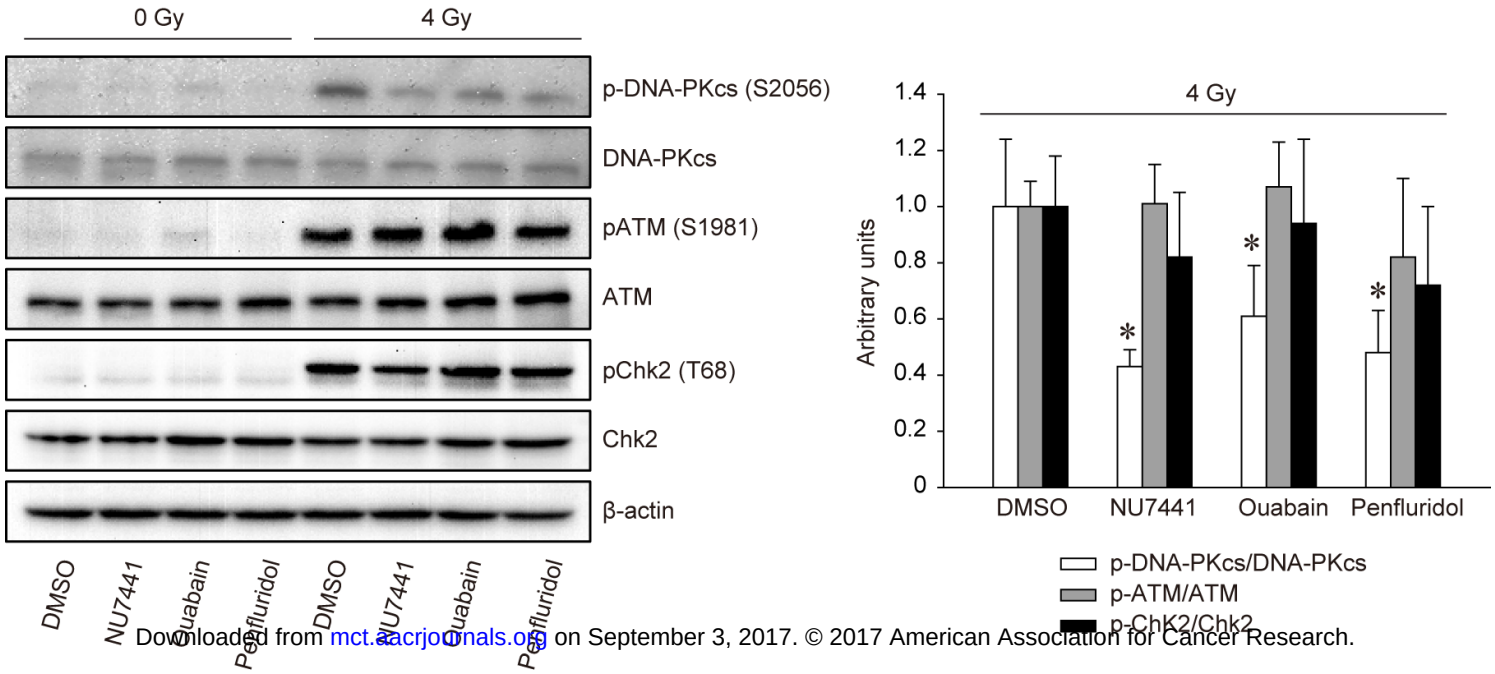

AACR American Association for Cancer Research

Molecular Cancer Therapeutics

A CRISPR/Cas9-based screening for non-homologous end joining inhibitors reveals ouabain and penfluridol as radiosensitizers

Jie Du, Jun Shang, Fei Chen, et al.

Mol Cancer Ther Published OnlineFirst September 1, 2017.